Research Article | Vol. 28, No. 16 / 3 August 2020 / Optics Express 23820
Optics EXPRESS

Optically tunable grating in a $V + \Xi$ configuration involving a Rydberg state

JINPENG YUAN,[1,2] SHICHAO DONG,[1,2] CHAOHUA WU,[1,2,3] LIRONG WANG,[1,2,*] LIANTUAN XIAO,[1,2] AND SUOTANG JIA[1,2]

[1] State Key Laboratory of Quantum Optics and Quantum Optics Devices, Institute of Laser Spectroscopy, Shanxi University, 92 Wucheng Road, Taiyuan 030006, China
[2] Collaborative Innovation Center of Extreme Optics, Shanxi University, 92 Wucheng Road, Taiyuan 030006, China
[3] Collaborative Innovation Center of Light Manipulations and Applications, Shandong Normal University, Jinan 250358, China
[*] wlr@sxu.edu.cn

Abstract: A novel tunable all-optical grating is realized experimentally in a $V + \Xi$ configuration coherent rubidium thermal vapor. This new energy level structure employs a Rydberg level as the uppermost level and contains two typical electromagnetically induced transparency energy level configurations with the same probe field. Compared with the traditional V-type three-level grating, a significant improvement of the diffraction efficiency of this novel grating was observed. Its improvement was then also demonstrated experimentally by the transition spectrum and theoretically by a comprehensive simulation. The diffraction efficiency gain introduced by the control laser field was tuned with several experimental parameters, such as the atomic density and the control field intensity. And the maximum enhancement rate of first-order diffraction efficiency is proved to be as high as 30%. Such a novel all-optical tunable grating promises to be the new driving force in the advancement of all-optical communications and information technology.

1. Introduction

The artificial dielectric structures with the ability of engineering the electromagnetic modes by the periodic and random changes in the refractive index, are playing and will continue to play a significant role in developing of optical communication [1,2], controlling light propagation behavior [3,4], synthetic optical devices and structures [5] and non-Hermitian quantum mechanics [6,7]. The "real" periodic optical structures, known as photonic crystals, have been studied for more than two decades [8]. The ability of periodic modulation the refractive index can fundamentally change the nature of light propagation in such materials, the photonic crystal related devices can, therefore, offer a flexible way to control the propagation of light [9]. The other "unreal" periodic optical structure known as optical induced atomic lattice, can play the same role but with more beneficial advantages. Coherent preparation by laser field of quantum states of atoms can lead to quantum interference, which will modify the medium optical properties, resulting in electromagnetically induced transparency (EIT) and related coherent effects [10]. Compared with the solid-state systems, the optical induced atomic lattice has the novel characters of flexible tunability, easy reconfiguration and especially the various coherence control techniques supported by the EIT.

Specially, when the travelling coupling field of a EIT configuration is replaced with a standing-wave mode, the absorption and dispersion of the probe laser beam in an atomic medium experienced a spatial modulation, which is referred to electromagnetically induced gratings (EIG). In compare with the traditional optical grating, the EIG configuration is easier to reconstruct and can be flexibly tuned to control the dynamic behavior of light propagation. EIG has numerous

#400618 https://doi.org/10.1364/OE.400618
Journal © 2020 Received 22 Jun 2020; revised 19 Jul 2020; accepted 22 Jul 2020; published 27 Jul 2020

Optics EXPRESS

applications in the realizations of all-optical device [11,12], photonic topological insulators [13], formation of vector dipole solitons [14] and simulation of non-Hermitian physics [15]. The first experimental realization of EIG is conducted in cold sodium atoms with a three-level Λ-type system [16]. The diffraction pattern of the laser propagated through the EIG was studied in thermal atom system [17–19]. Recently, the researches about the optical induced lattice or related applications have been extended to multi-dimensional and show more promising prospects [20–24].

While finding schemes to promote the diffraction efficiency of EIG is a main concern and lays a solid foundation for realizing the related applications. Many convincing theoretical mechanisms have been proposed in various energy level systems, such as Λ-type configuration [25], *N*-type configuration [26], ladder-type [27], *Y*-type [28] and four-level double-Λ atomic system [29]. At the same time, the Rydberg atom is considered as a powerful candidate for quantum optics research for its long radiative lifetime, large dipole moment and weak binding energies [30]. Introducing the Rydberg atom to EIG's research can combine the advantages of both and provides a prospect to achieve a more practical all-optical grating with strong optical nonlinearities. Just recently, the theoretical schemes about Rydberg atoms related EIG were extensively proposed [31–35], however, there is no experimental reports to our best knowledge so far. Because of the flexible tunable characteristics and complex dynamics of Rydberg EIT ensembles, many interesting questions remain open in experimental research about EIG involved Rydberg states.

In this work, we obtain an all-optical tunable EIG by devising a feasible and innovative scheme. A four-level atomic configuration using the Rydberg state as the uppermost level is employed, two types of *V*- and Ξ-type EIT configurations are involved with the same probe field. As a significant result, we find that the diffraction efficiency of this all-optical grating is highly enhanced in each order directions compared with the three-level case. It is shown that the experimental parameters, such as the atomic density and control laser intensity, have an appreciable effect on enhancing the intensity of diffraction orders. To further understand these results, a comprehensive theoretical simulation is also given. Our work not only provides opportunities for the realization of background-free atomic gratings, but because of the presence of Rydberg atoms with strong dipole-dipole interaction, it provides solutions for the practical realization of quantum imaging and signal processing at a microscopic scale [32]. This novel grating may also open a potential way to all-optical communications and the optical quantum devices.

2. Experimental setup

The schematic of the energy levels employed in this experiment is shown in Fig. 1(a). Three laser fields are involved to construct two EIT configurations with *V*- and Ξ-type simultaneously. A strong switching field with Rabi frequency Ω_s coupling the $5S_{1/2}$ (F=3) ($|1\rangle$)-$5P_{1/2}$ (F =3) ($|2\rangle$) hyperfine transition is used to construct the standing-wave field. A weak probe field with Rabi frequency Ω_p corresponding to the $5S_{1/2}$ (F =3) -$5P_{3/2}$ (F=4) ($|3\rangle$) hyperfine transition is used to observe the diffraction patterns. A control laser field with Rabi frequency Ω_c coupling the $5P_{3/2}$ (F=4) state and the uppermost Rydberg state $57D_{5/2}$ ($|4\rangle$) is introduced to provide a controllable improvement of diffraction efficiency.

The sketch of the experiment system is illustrated in Fig. 1(b). The switching and probe laser beams corresponding to 795 nm and 780 nm are all provided by two external cavity diode lasers (DL pro, Toptica). The frequencies of these two lasers are locked by saturation absorption spectroscopy method. A wavelength meter (WS-7, HighFinesse) is used to monitor the laser frequency. The switching beam is firstly shaped by an anamorphic prism pair with the result of an elliptical profile. Then, the elliptical beam passing through a beam-splitter to obtain two beams with the same profile and power. And the two beams are recombined symmetrically again in the center of a rubidium vapor cell with a small angle $2\varphi \approx 0.4$ degrees. A standing-wave field appears perpendicular to the propagation direction of the probe field with a grating constant

Optics EXPRESS

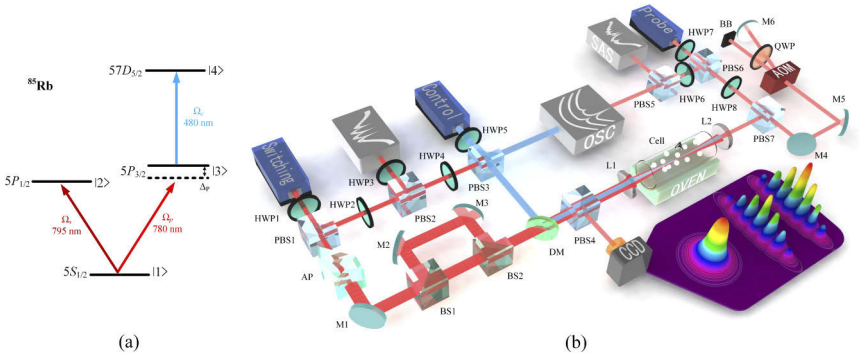

Fig. 1. (a) Energy levels of a ($V + \Xi$)-type ^{85}Rb atomic system. (b) Experimental setup. HWP, half-wave plate; PBS, polarization beam splitter; AP, anamorphic prism; M, high reflection mirror; BS, beam splitter; DM, dichroic mirror; CCD, charge-coupled device; L, lens; SAS, saturation absorption spectroscopy; OSC, oscilloscope; BB, beam block; QWP, quarter-wave plate; AOM, acousto-optic modulator.

of $\Lambda_x = \lambda_s/(2\sin\varphi)$, where λ_s is the wavelength of the switching laser. The vapor cell with a length of 10 cm is wrapped with a μ-metal sheet to shield the magnetic field and precisely temperature controlled by two ceramics heater. A double-pass system of acousto-optic modulator is introduced to accurately tune the frequency of the probe laser without changing the propagation direction. The probe laser propagates through the EIG and will be diffracted into high order patterns. A charge-coupled device (CCD) is employed to record the diffraction pattern of the probe laser in real time.

Then the control laser (TA-SHG pro, Toptica) corresponding to 480 nm with travelling mode is introduced into the three-level V-type EIG. The frequency lock of the laser is achieved by the EIT spectroscopy. It is worth noting that a control field with high laser intensity is needed to overcome the lower transition probability between the employed energy levels. A clearly distinguishable diffraction gain is brought into this novel EIG configuration and studied in the following.

3. Experimental results and discussions

Applying the rotating wave approximation, the interaction Hamiltonian of the system can be written as

$$H_I = \frac{\hbar}{2}[\Omega_p|1\rangle\langle 3| + \tilde{\Omega}_s|1\rangle\langle 2| + \Omega_c|3\rangle\langle 4|] + \hbar[\Delta_p|3\rangle\langle 3| + \Delta_s|2\rangle\langle 2| + (\Delta_p + \Delta_c)|4\rangle\langle 4|] + h.c., \quad (1)$$

where $\Delta_p = \omega_p - \omega_{31}$, $\Delta_s = \omega_s - \omega_{21}$, $\Delta_c = \omega_c - \omega_{43}$ are the corresponding frequency detunings. Here, ω_p, ω_s and ω_c stand for the frequencies of probe, switching and control fields, respectively. In addition, ω_{ij} (i, j=1, 2, 3, 4) are the frequency differences between level $|i\rangle$ and level $|j\rangle$ and h.c. is the Hermitian conjugate. We assume the standing-wave field has a sinusoidal profile as $\tilde{\Omega}_s = \Omega_s \sin(\pi x/\Lambda_x)$.

The susceptibility of the probe field in this (V+Ξ)-type system can be obtained by $\chi = \frac{N|\mu_{31}|^2}{\varepsilon_0\hbar\Omega_p}\rho_{31}$, where N is the atomic density, μ_{31} is the transition dipole momentum between level $|3\rangle$ and $|1\rangle$, ε_0 is the permittivity of free space and ρ_{31} is the density-matrix element for the transition $|1\rangle \rightarrow |3\rangle$. By applying the density-matrix method, the steady-state solution for ρ_{31} is given by

$$\rho_{31} = \frac{i\Omega_p(\gamma_{23}\tilde{\Omega}_s^2 + \gamma_{41}\Omega_c^2 + 4\gamma_{23}\gamma_{41}\gamma_{42})}{\tilde{\Omega}_s^2\Omega_c^2 - \tilde{\Omega}_s^4 - \Omega_c^4 - 2\tilde{\Omega}_s^2(\gamma_{31}\gamma_{23} + \gamma_{41}\gamma_{42}) - 3\Omega_c^2(\gamma_{31}\gamma_{41} + \gamma_{23}\gamma_{42}) - 8\gamma_{31}\gamma_{23}\gamma_{41}\gamma_{42}}. \quad (2)$$

Optics EXPRESS

Here, $\gamma_{31} = -\frac{\Gamma_3}{2} + i\Delta_p$, $\gamma_{23} = -\frac{\Gamma_2+\Gamma_3}{2} - i(\Delta_s - \Delta_p)$, $\gamma_{41} = -\frac{\Gamma_4}{2} + i(\Delta_p + \Delta_c)$ and $\gamma_{42} = -\frac{\Gamma_4+\Gamma_2}{2} + i(\Delta_c + \Delta_p - \Delta_s)$. In addition, Γ_2, Γ_3 and Γ_4 are the decay rates from the upper levels. In the steady-state regime and under the slowly varying envelope approximation, the propagation of the probe field along the z direction using the Maxwell's equation can be described as

$$\frac{\partial E_p}{\partial z} = [\alpha + i\beta]E_p, \tag{3}$$

where $\alpha(x) = [\frac{2\pi}{\lambda}]\mathrm{Im}[\chi]$ and $\beta(x) = [\frac{2\pi}{\lambda}]\mathrm{Re}[\chi]$ are the absorption and dispersion coefficients of the probe field, respectively. By solving Eq. (2), the transmission function of the modulated probe field at $z = L$ can be calculated analytically and is given by

$$T(x) = e^{-\alpha(x)L + i\beta(x)L}, \tag{4}$$

where $e^{-\alpha(x)L}$ and $e^{i\beta(x)L}$ denote the absorption and phase modulation, respectively. Under the assumption that the input probe field is a plane wave, the diffraction intensity distribution can be expressed as

$$I(\theta) = |E(\theta)|^2 \times \frac{\sin^2(M\pi\Lambda_x \sin(\theta))/\lambda}{M^2 \sin^2(\pi\Lambda_x \sin(\theta)/\lambda)}, \tag{5}$$

where θ is the diffraction angle along the z direction, M denotes the number of the spatial period of the optical grating, and $E(\theta) = \int_0^{\Lambda_x} T(x)e^{-2\pi i\Lambda_x x \sin(\theta)/\lambda}dx$ denotes the Fraunhofer diffraction of a single period.

The nth-order diffraction is determined by the grating equation and the diffraction order n is defined as $n = (\frac{\Lambda_x \sin(\theta)}{\lambda})$, where $n = 0, 1, 2, 3, \ldots$ is the diffraction order. So, the nth-order intensity diffraction equation can be expressed as

$$I(\theta_n) = |E(\theta_n)|^2 = |\int_0^1 T(x)e^{-2n\pi ix}dx|^2. \tag{6}$$

We numerically simulate the diffraction patterns in this grating configuration and the traditional V case by normalizing the above theoretical results, which are shown in Fig. 2. The red dashed curve is plotted with the Rabi frequency of the control field is $\Omega_c = 0$, thus the result shows the behavior of a typical V-type system, while the blue curve corresponds to this ($V + \Xi$)-type system with $\Omega_c = 1.5\Gamma_3$. It can be seen that the diffraction efficiency in this novel grating has a significant improvement compared with the traditional V-type three-level case.

The transition spectra and diffraction patterns for these two configurations under various conditions are shown in Fig. 3. The transmission spectra of the probe laser passing through the vapor cell is illustrated in Fig. 3(a). When we scan the laser frequency over $5S_{1/2}$ (F=3)-$5P_{3/2}$ transition, a clear Doppler background is obtained. When a switching laser field resonances with the hyperfine transition of $5S_{1/2}$ (F = 3)-$5P_{1/2}$ (F′ = 3) is propagating through the vapor in opposite direction of the probe field, a typical EIT spectrum is observed in Fig. 3(b). Figure 3(c) shows the transmission spectra of the probe field when the control laser is introduced in the system, and the laser frequency corresponding to $5P_{3/2}$ (F = 4) - $57D_{5/2}$ transition. Because of the narrow frequency interval between $57D_{5/2}$ state and $57D_{3/2}$ state, there is an extra small peak corresponding to $5S_{1/2}$-$5P_{3/2}$-$57D_{3/2}$ transition. The transition spectra of the cases (a) and (b) are also referenced in the Fig. 3(c) with dashed lines. It is obvious that in the absence of the control laser, an absorption peak appears corresponding to the absorption of the typical V-type EIT. While with an additional control laser introducing, the amplitude of the transition peak has undergone an obvious improvement, which is considered to be about five times. Thus, we expect that for a combined $V + \Xi$ configuration system, the intensity of the diffraction patterns will be enhanced significantly.

Optics EXPRESS

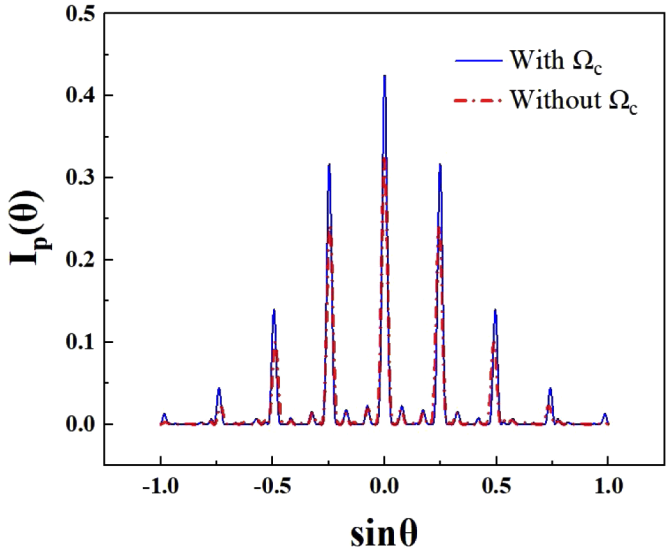

Fig. 2. The theoretical simulation of the diffraction patterns in V-type (red dashed curve) and ($V + \Xi$)-type (blue curve) systems. In this figure, $\Delta_s = \Delta_c = 0$, $\Delta_p = 0.5\Gamma_3$, $\Omega_s = \Gamma_3$, in red dashed curve $\Omega_c = 0$ and in blue curve $\Omega_c = 1.5\Gamma_3$.

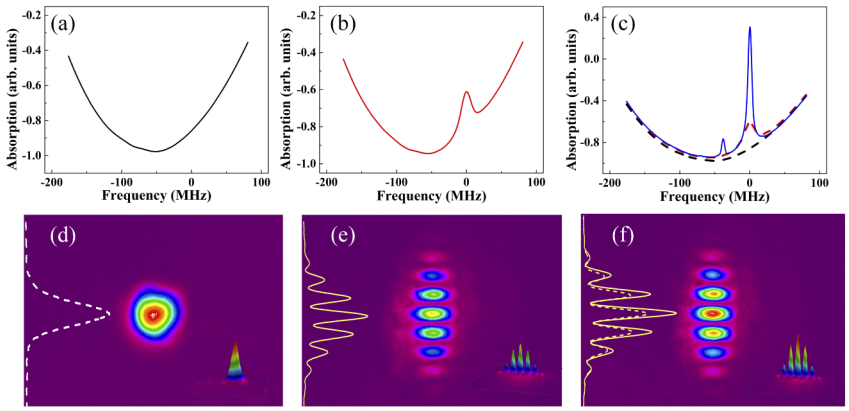

Fig. 3. (a) The Doppler absorption spectroscopy of the probe laser corresponding to $5S_{1/2}$ (F = 3)-$5P_{3/2}$ transition. (b) The EIT spectroscopy with switching laser locked on $5S_{1/2}$ (F = 3)- $5P_{1/2}$ (F = 3) hyperfine transition. (c) The EIT spectroscopy (blue solid curve) with control laser introduced in, where figures (a) (black dashed curve) and (b) (red dashed curve) are also referenced. (d) The profile of the incident probe laser. (e) The diffraction pattern of the V-type EIG. (f) The diffraction pattern of the ($V + \Xi$)-type EIG. In (d-f), the curves represent the intensity distributions of the diffraction patters and the insets are the corresponding three-dimensional profiles.

Figure 3(d) is the experimentally observed profile of the probe beam propagated through the vapor, the inset is the corresponding three-dimensional distribution. The white dashed curve depicts its intensity profile, which shows a typical Gaussian beam. When a standing-wave switching field constructed by the interference of two switching lasers acts on the atomic vapor, a V-type EIG is formed. The strong standing-wave field will bring a spatial periodic modulation to the atomic medium refractive index, which will result in a far-field Fraunhofer diffraction effect

Optics EXPRESS

when the weak probe field propagates through the medium. Figure 3(e) is the diffraction profile after the probe beam propagated through this V-type EIG. Third- and even fourth-order diffraction patterns are distinguishably observed. The relevant experimental parameters are as follows, the probe laser has a power of 5 mW and its frequency is blue detuned 20 MHz to $5S_{1/2}$ (F = 3)-$5P_{3/2}$ (F = 4) hyperfine transition, the temperature of vapor cell is 116 °C. Here the introduced phase modulation for the two-photon detuning serves as a nontrivial control knob, which can avoid the limitation of pure amplitude modulation on high-order diffraction efficiency [36]. This frequency detuning ensures large grating diffraction efficiencies of each orders. The switching laser power is 12 mW and its frequency resonances with hyperfine transition of $5S_{1/2}$ (F = 3) - $5P_{1/2}$ (F′ =3). Further, a combined (V + Ξ)-type EIG configuration is achieved by introducing a control laser. The control laser resonances with $5P_{3/2}$ (F=4) - $57D_{5/2}$ transition has a power of 540 mW. The diffraction pattern in this novel configuration is shown in Fig. 3(f). It is observed that the intensity of the combined (V + Ξ)-type system is larger than that for a simple V-type system in each diffraction orders. Here a visible diffraction enhancement effect can only be observed with control laser power exceeds 120 mW, which is owed to the low transition probability between the intermediate state and the Rydberg energy level. Therefore, this mechanism can be used to improve the efficiency of the all-optical grating.

By using the advantages of this multi-parameter system, we can tune this enhancement rate by adjusting the atomic density and control laser power. Atomic density is precisely determined by the temperature of the vapor. We measured the diffraction patterns with different vapor temperatures as shown in Fig. 4(a). The powers of the control, switching and probe lasers are 540 mW, 12 mW and 5 mW, respectively. The temperature of the atomic vapor is varied from 104 °C to 118 °C, which corresponding to atomic densities of 7.75×10^{12} cm^3 to 1.81×10^{13} cm^3. The enhancement effect is more obvious as the temperature increases. This is reflected not only in the diffraction intensity, but also in the diffraction order. The first-order diffraction efficiency enhancement rate of the (V + Ξ)-type configuration compare with V-type EIG is also shown in Fig. 4(b). The dots are the averaged experimental results of three times and the errors are the standard deviation. The diffraction efficiency is defined as the ratio of the intensity of the selected diffraction beam to the incident beam. The enhancement rate is characterized as $\kappa = \frac{\eta_{(V+\Xi)} - \eta_V}{\eta_V}$, where $\eta_{(V+\Xi)}$ and η_V are the first diffraction efficiencies of the corresponding configurations, respectively. As a result, the enhancement rate is found to increase with increasing temperature. It can be seen from the theoretical simulation that the susceptibility of this atomic system is affected by the atomic density. Atomic density increases with increasing temperature, which will lead to a larger refractive index contrast. However, if the atomic density is too large, the absorption of the probe laser becomes significant, which will reduce the diffraction intensity of each orders.

Also, the diffraction efficiency of this all-optical grating can be tuned by the control field intensity. Figures 5(a)–(f) show the three-dimensional output diffraction patterns with different control laser powers. The powers of the switching and probe lasers are the same as Fig. 4. The temperature of the vapor is fixed at 116 °C, which corresponding to an atomic density of 1.61×10^{13} cm^3. The number of diffraction orders keeps the same, but the diffraction efficiency of each order has a significant enhancement with the increase of control laser power. The control field pumps the atoms population from lower level $5P_{3/2}$ (F=4) to upper level $57D_{5/2}$, and the Rydberg-EIT plays a vital rule in improving the diffraction efficiency, because large dispersion is accompanied by weaker absorption [33]. Figure 5(g) shows the more detailed continuous change trend of the diffraction intensity distribution with different control laser powers. It can be seen that by increasing the power of the control field, the first-order diffraction intensity increases almost linearly, and then reaches the maximum value. In order to quantify this effect,we give the enhancement rate in first-order diffraction efficiency, which is shown in Fig. 5(h). It can be observed that increasing the control laser power leads to higher diffraction efficiency

Optics EXPRESS

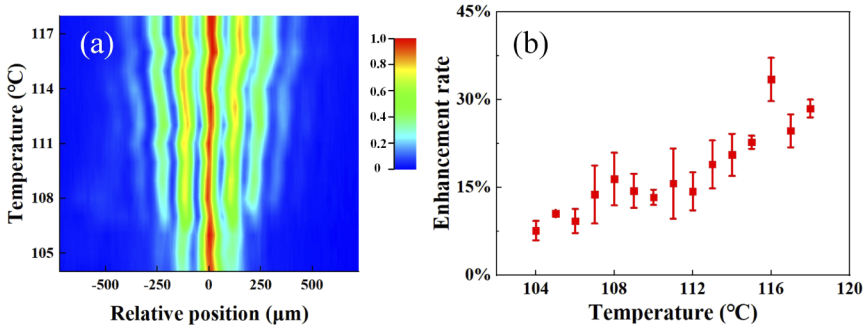

Fig. 4. (a)The intensity distributions of diffraction patterns with different vapor temperatures. (b) The first-order diffraction efficiency enhancement rate versus atomic vapor temperature. The error bar is the standard deviation of three experiment measurements.

enhancement. But as power continues to increase, the saturation effect is observed. This trend is basically consistent with the theoretical simulation, which predicts that the gain first increases with control laser intensity, then reaches saturation, and finally decreases with further increase in control laser intensity. Physically speaking, the nodes and antinodes of the standing-wave will be more distinct by increasing Ω_c, and EIT will open a better transparency window. Therefore, more probe light will be available for diffraction, so the diffraction intensity will be improved. After the maximum value, the increase of the Rabi frequency of the control field leads to a huge nonlinearity in the atomic medium and destroys the EIT condition. Therefore, in the case of a larger control field strength, since the probe energy can be efficiently transferred to the higher

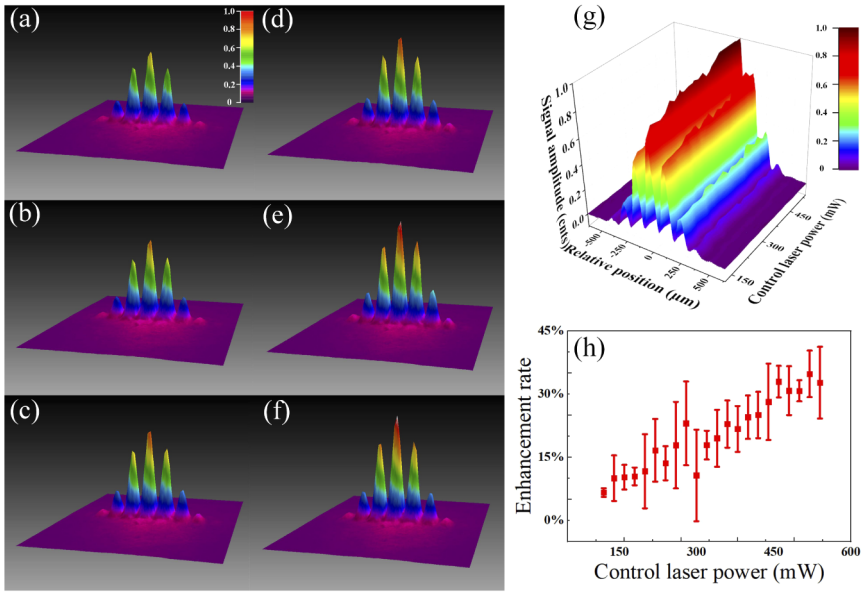

Fig. 5. The three-dimensional diffraction patterns with control laser powers of (a) 120 mW, (b) 200 mW, (c) 280 mW, (d) 360 mW, (e) 440 mW (f) 520 mW. (g) The corresponding diffraction intensity distributions with control laser powers varied from 120 mW to 540 mW with an interval of 20 mW. (h) The first-order diffraction efficiency enhancement rate versus different control laser power.

Optics EXPRESS

order direction and deviate from the original propagation direction, the grating also provides a further possibility of all-optical beam splitting.

4. Conclusions

In summary, we have experimentally studied an all-optical EIG in a four-level ($V+\Xi$)-type atomic system, which includes a Rydberg state as the uppermost level. A significant improvement of the diffraction efficiency of this novel grating was found compared with the traditional V-type three-level grating. The improvement effect can be tuned by the atomic density and the control field intensity, and the results all show a positive correlation trend. This nonlinear and large diffraction efficiency gain is demonstrated experimentally for the first time. And the maximum enhancement rate of first-order diffraction efficiency is found to be as high as 30 %. With Rydberg atoms introducing in the artificial dielectric structure of electromagnetically induced grating, the advantages of these two have dramatic results. This system provides a unique platform to take advantage of the strong optical nonlinearity of Rydberg atoms, and it can bring to the development of all-optical quantum device.

Funding

National Key Research and Development Program of China (2017YFA0304203); National Natural Science Foundation of China (61705122, 61875112, 91736209); Program for Sanjin Scholars of Shanxi Province; Key Research and Development Program of Shanxi Province for International Cooperation (201803D421034); 1331KSC.

Disclosures

The authors declare no conflicts of interest.

References

1. W. B. Gao, A. Imamoglu, H. Bernien, and R. Hanson, "Coherent manipulation, measurement and entanglement of individual solid-state spins using optical fields," Nat. Photonics **9**(6), 363–373 (2015).
2. D. D. Awschalom, R. Hanson, J. Wrachtrup, and B. B. Zhou, "Quantum technologies with optically interfaced solid-state spins," Nat. Photonics **12**(9), 516–527 (2018).
3. M. Bajcsy, A. S. Zibrov, and M. D. Lukin, "Stationary pulses of light in an atomic medium," Nature **426**(6967), 638–641 (2003).
4. J. Everett, G. T. Campbell, Y.-W. Cho, P. Vernaz-Gris, D. B. Higginbottom, O. Pinel, N. P. Robins, P. K. Lam, and B. C. Buchler, "Dynamical observations of self-stabilizing stationary light," Nat. Phys. **13**(1), 68–73 (2017).
5. H. Hodaei, M.-A. Miri, M. Heinrich, D. N. Christodoulides, and M. Khajavikhan, "Parity-time-symmetric microring lasers," Science **346**(6212), 975–978 (2014).
6. H. Hodaei, A. U. Hassan, S. Wittek, H. Garcia-Gracia, R. El-Ganainy, D. N. Christodoulides, and M. Khajavikhan, "Enhanced sensitivity at higher-order exceptional points," Nature **548**(7666), 187–191 (2017).
7. R. El-Ganainy, K. G. Makris, M. Khajavikhan, Z. H. Musslimani, S. Rotter, and D. N. Christodoulides, "Non-Hermitian physics and PT symmetry," Nat. Phys. **14**(1), 11–19 (2018).
8. J. D. Joannopoulos, S. G. Johnson, J. N. Winn, and R. D. Meade, *Photonic Crystals: Molding the Flow of Light*, 2nd ed. (Princeton University, 2008).
9. R. M. De La Rue and C. Seassal, "Photonic crystal devices: some basics and selected topics," Laser Photonics Rev. **6**(4), 564–597 (2012).
10. M. Fleischhauer, A. Imamoglu, and J. P. Marangos, "Electromagnetically induced transparency: Optics in coherent media," Rev. Mod. Phys. **77**(2), 633–673 (2005).
11. A. W. Brown and M. Xiao, "All-optical switching and routing based on an electromagnetically induced absorption grating," Opt. Lett. **30**(7), 699–701 (2005).
12. L. Zhao, W. Duan, and S. F. Yelin, "All-optical beam control with high speed using image-induced blazed gratings in coherent media," Phys. Rev. A **82**(1), 013809 (2010).
13. Y. Zhang, Z. Wu, M. R. Belia, H. Zheng, Z. Wang, M. Xiao, and Y. Zhang, "Photonic floquet topological insulators in atomic ensembles," Laser Photonics Rev. **9**(3), 331–338 (2015).
14. Y. Zhang, Z. Wang, Z. Nie, C. Li, H. Chen, K. Lu, and M. Xiao, "Four-wave mixing dipole soliton in laser-induced atomic gratings," Phys. Rev. Lett. **106**(9), 093904 (2011).

Optics EXPRESS

15. Y. Liu, F. Gao, J. Wu, M. Artoni, and G. C. La Rocca, "Lopsided diffractions of distinct symmetries in two-dimensional non-hermitian optical gratings," Phys. Rev. A **100**(4), 043801 (2019).
16. M. Mitsunaga and N. Imoto, "Observation of an electromagnetically induced grating in cold sodium atoms," Phys. Rev. A **59**(6), 4773–4776 (1999).
17. J. Sheng, J. Wang, M.-A. Miri, D. N. Christodoulides, and M. Xiao, "Observation of discrete diffraction patterns in an optically induced lattice," Opt. Express **23**(15), 19777–19782 (2015).
18. J. Yuan, Y. Li, S. Li, C. Li, L. Wang, L. Xiao, and S. Jia, "Experimental study of discrete diffraction behavior in a coherent atomic system," Laser Phys. Lett. **14**(12), 125206 (2017).
19. J. Yuan, C. Wu, Y. Li, L. Wang, Y. Zhang, L. Xiao, and S. Jia, "Integer and fractional electromagnetically induced talbot effects in a ladder-type coherent atomic system," Opt. Express **27**(1), 92–101 (2019).
20. Z. Zhang, F. Li, G. Malpuech, Y. Zhang, O. Bleu, S. Koniakhin, C. Li, Y. Zhang, M. Xiao, and D. D. Solnyshkov, "Particlelike behavior of topological defects in linear wave packets in photonic graphene," Phys. Rev. Lett. **122**(23), 233905 (2019).
21. H. Cai, J. Liu, J. Wu, Y. He, S.-Y. Zhu, J.-X. Zhang, and D.-W. Wang, "Experimental observation of momentum-space chiral edge currents in room-temperature atoms," Phys. Rev. Lett. **122**(2), 023601 (2019).
22. J. Yuan, C. Wu, L. Wang, G. Chen, and S. Jia, "Observation of diffraction pattern in two-dimensional optically induced atomic lattice," Opt. Lett. **44**(17), 4123–4126 (2019).
23. Z. Zhang, R. Wang, Y. Zhang, Y. V. Kartashov, F. Li, H. Zhong, H. Guan, K. Gao, F. Li, Y. Zhang, and M. Xiao, "Observation of edge solitons in photonic graphene," Nat. Commun. **11**(1), 1902 (2020).
24. Z. Zhang, S. Liang, F. Li, S. Ning, Y. Li, G. Malpuech, Y. Zhang, M. Xiao, and D. Solnyshkov, "Spin-orbit coupling in photonic graphene," Optica **7**(5), 455–462 (2020).
25. T. Shui, W.-X. Yang, S. Liu, L. Li, and Z. Zhu, "Asymmetric diffraction by atomic gratings with optical $\mathcal{PT}$ symmetry in the Raman-Nath regime," Phys. Rev. A **97**(3), 033819 (2018).
26. V. G. Arkhipkin and S. A. Myslivets, "One- and two-dimensional raman-induced diffraction gratings in atomic media," Phys. Rev. A **98**(1), 013838 (2018).
27. F. Bozorgzadeh, M. Sahrai, and H. Khoshsima, "Controlling the electromagnetically induced grating via spontaneously generated coherence," Eur. Phys. J. D **70**(9), 191 (2016).
28. T. Naseri and R. Sadighi-Bonabi, "Electromagnetically induced phase grating via population trapping condition in a microwave-driven four-level atomic system," J. Opt. Soc. Am. B **31**(11), 2879–2884 (2014).
29. T. Shui, W.-X. Yang, L. Li, and X. Wang, "Lop-sided Raman-Nath diffraction in $\mathcal{PT}$-antisymmetric atomic lattices," Opt. Lett. **44**(8), 2089–2092 (2019).
30. M. Saffman, T. G. Walker, and K. Malmer, "Quantum information with Rydberg atoms," Rev. Mod. Phys. **82**(3), 2313–2363 (2010).
31. T. Naseri, "Two-dimensional induced grating in Rydberg atoms via microwave field," Eur. Phys. J. Plus **134**(10), 530 (2019).
32. S. Asghar Ziauddin, S. Qamar, and S. Qamar, "Electromagnetically induced grating with Rydberg atoms," Phys. Rev. A **94**(3), 033823 (2016).
33. F. Bozorgzadeh and M. Sahrai, "All-optical grating in a $V + \Xi$ configuration using a Rydberg state," Phys. Rev. A **98**(4), 043822 (2018).
34. D. Ma, D. Yu, X.-D. Zhao, and J. Qian, "Unidirectional and controllable higher-order diffraction by a Rydberg electromagnetically induced grating," Phys. Rev. A **99**(3), 033826 (2019).
35. C. Hang, W. Li, and G. Huang, "Nonlinear light diffraction by electromagnetically induced gratings with $\mathcal{PT}$ symmetry in a Rydberg atomic gas," Phys. Rev. A **100**(4), 043807 (2019).
36. J. Yuan, C. Wu, Y. Li, L. Wang, Y. Zhang, L. Xiao, and S. Jia, "Controllable electromagnetically induced grating in a cascade-type atomic system," Front. Phys. **14**(5), 52603 (2019).